



## OPEN A recombinant BCG with surface-displayed antigen induces humoral and cellular immune responses

Jin-Yu Zhang<sup>1</sup>, Zhi-Dong Hu<sup>2</sup>, Li-Xiao Xing<sup>1</sup>, Zhen-Yan Chen<sup>2</sup>, Jin-Chuan Xu<sup>2</sup>, Qiao-Yu Wu<sup>2</sup>, Juan Wu<sup>2</sup>, Guo-Ping Zhao<sup>1,3,4</sup>, Xiao-Yong Fan<sup>2,5</sup> & Liang-Dong Lyu<sup>1,6</sup>

*Bacillus Calmette-Guérin* (BCG) is an attenuated vaccine widely used for tuberculosis prevention. While BCG has long been perceived as an intracellular candidate vector for delivering antigens against infectious diseases and cancers, challenges persist in inducing durable immune responses, particularly high-titer neutralizing antibodies (Nabs). Here we show that displaying antigens in the surface of BCG is a promising strategy to induce long-lasting Nabs production and T-cell responses. We constructed a recombinant BCG expressing the SARS-CoV-2 receptor-binding domain (RBD) antigen on its cell wall, termed CW-rBCG::RBD, which achieved an antigen yield approaching 850 nanograms per 10<sup>7</sup> colony-forming unit. Compared with both the parental BCG and the RBD protein subunit vaccine (RBD<sup>AS01</sup>), intravenous administration of CW-rBCG::RBD followed by a booster dose significantly enhanced Nab production and increased the frequencies of RBD-specific central memory T cells (T<sub>cm</sub>) and T follicular helper (T<sub>fh</sub>) cells in the spleen. In mice primed with a single dose of CW-rBCG::RBD and boosted with RBD<sup>AS01</sup>, we also observed elevated Nab titers and detectable levels of RBD-specific IgG2a antibodies at 8 weeks post-priming, responses that were not observed in the BCG-primed or RBD<sup>AS01</sup>-only groups. Furthermore, subcutaneous co-administration of CW-rBCG::RBD and RBD<sup>AS01</sup> sustained Nab production for up to 31 weeks and maintained higher T<sub>fh</sub> and T<sub>cm</sub> cell frequencies compared to both BCG co-administration with RBD<sup>AS01</sup> and RBD<sup>AS01</sup> alone. These findings highlight an effective strategy for optimizing BCG-based vaccination and immunotherapy platforms. **Subject terms:** recombinant BCG; immune response; vaccines; cell wall; SARS-CoV-2 RBD.

*Bacillus Calmette-Guérin* (BCG), an attenuated strain of *Mycobacterium bovis*, is widely used as a tuberculosis vaccine and has gained attention as a vector for delivering antigens against infectious diseases and cancers due to its safety, intracellular persistence, and strong immune-stimulatory properties. These characteristics enable BCG to prolong antigen exposure and activate both innate and adaptive immune responses.

Recombinant BCG (rBCG) strains have been developed to express heterologous antigens, showing promise in inducing antigen-specific T cell responses in models of cancer and infections, such as bladder cancer<sup>1</sup> and breast cancer<sup>2</sup>, as well as for infectious diseases such as Human Immunodeficiency Virus (HIV), human Respiratory Syncytial Virus (RSV), human Metapneumovirus (hMPV), Hepatitis C Virus (HCV) and Simian Immunodeficiency Virus (SIV)<sup>3-7</sup>. Recombinant BCG (rBCG) strains have shown potential in eliciting T cell activation in mouse models. For instance, rBCG expressing hMPV antigens has been shown to induce a Th1 response<sup>7</sup>, rBCG expressing HCV antigens can elicit CD8<sup>+</sup> T cell activation<sup>4</sup>. Despite ongoing efforts, rBCG has had limited success in inducing robust humoral responses, particularly the generation of neutralizing antibodies (Nabs)<sup>3-8</sup>. Although T cell responses can support B cells in producing antibodies, they are generally insufficient to induce a robust and sustained humoral response independently<sup>9</sup>. Recent study, however, has shown that when BCG is used as an adjuvant, it can significantly enhance humoral responses when combined with SARS-CoV-2 subunit vaccines<sup>10</sup>.

<sup>1</sup>Key Laboratory of Medical Molecular Virology of the Ministry of Education/National Health Commission, School of Basic Medical Sciences and Department of Microbiology and Microbial Engineering, School of Life Sciences, Fudan University, Shanghai, China. <sup>2</sup>Shanghai Public Health Clinical Center, Fudan University, Shanghai, China. <sup>3</sup>Key Laboratory of Synthetic Biology, Institute of Plant Physiology and Ecology, Shanghai Institutes for Biological Sciences, Chinese Academy of Science, Shanghai 200032, China. <sup>4</sup>Shanghai-MOST Key Laboratory of Health and Disease Genomics, Chinese National Human Genome Center at Shanghai, Shanghai 201203, China. <sup>5</sup>Shanghai Institute of Infectious Diseases and Biosecurity, Fudan University, Shanghai, China. <sup>6</sup>Shanghai Key Laboratory of Tuberculosis, Shanghai Clinical Research Center for Infectious Disease (Tuberculosis), Shanghai Pulmonary Hospital, Shanghai, China. ✉email: gpzhao@sibs.ac.cn; xyfan008@fudan.edu.cn; ld.lyu@fudan.edu.cn

T follicular helper (Tfh) cells, a subset of CD4<sup>+</sup> T cells, are crucial for B cell affinity maturation and durable antibody responses<sup>11,12</sup>. Previous research has highlighted that the formulation of BCG and RBD subunit vaccines enhances antibody responses, emphasizing the critical role of T cell responses in supporting antibody production<sup>10</sup>. This is further evidenced by improved humoral responses when BCG priming is followed by boosting with non-homologous vaccine expressing *M. tb* antigens<sup>13</sup>. However, in the context of emerging viral threats like COVID-19, rBCG expressing SARS-CoV-2 nucleoprotein (N) has shown limited ability to induce Tfh cells and humoral responses<sup>14</sup>. The exact mechanisms by which rBCG induces antigen-specific humoral responses remain unclear.

The lipoprotein antigens of *M. tb* are abundantly present in the cell wall and cell membrane<sup>15,16</sup>. rBCG expressing *M. tb* lipoprotein antigens has been associated with enhanced T cell responses and improved protection against *M. tb* infection<sup>17</sup>. These lipoproteins are recognized by T cells and presented by MHC class I molecules, which leads to the activation of CD8<sup>+</sup> T cells, crucial for viral protection<sup>18</sup>. Furthermore, antibodies targeting these lipoproteins have been detected in *M. tb*-infected individuals<sup>19</sup>. The immunogenicity of *M. tb* lipoproteins may be attributed to their localization of cell wall and membrane, facilitating early and efficiently interaction with antigen-presenting cells (APCs). Individuals infected with *M. tb* maintain B cells that predominantly target lipoprotein epitopes, and these B cells are capable of antibody production<sup>20</sup>. APCs, including B cells, may directly recognize cell wall-associated antigens. These B cells not only present antigens but can also secrete specific antibodies targeting the surface antigens they encounter<sup>20</sup>. This suggests that rBCG displaying antigens on its cell wall may enhance humoral responses by facilitating efficient antigen recognition and presentation, contributing to sustained antibody production. Most previous rBCG construction strategies have focused on maximizing antigen expression within the cytosol or secretory pathways, with little emphasis on antigen localization<sup>3–5,8–10</sup>. The potential of directing antigens to the BCG cell surface—where they are more accessible to B cell receptors and T cell and thus more likely to initiate strong antibody responses—has not been fully explored.

Here, we report the development of CW-rBCG::RBD, a recombinant strain that displays the SARS-CoV-2 receptor-binding domain (RBD) on its cell wall. This approach significantly enhanced RBD-specific Nabs and Tfh cell responses compared to parent BCG and RBD subunit vaccines. Intravenous administration of CW-rBCG::RBD induced durable central memory T cells (Tcm) cell responses and RBD-specific Tfh cell responses, accompanied by higher Nab titers. Co-administration with an RBD subunit vaccine further extended Nab production. These findings suggest that cell wall-displayed antigens on BCG could effectively enhance humoral responses, offering a promising approach for improving rBCG vaccine, particularly in the context of long-term immunity.

## Results

### Expression of SARS-CoV-2 RBD protein on the cell wall of Recombinant BCG

The 19-kilodalton (KD) antigen, a well-characterized lipoprotein from *M. tuberculosis* (encoded by *Rv3763*), predominantly localized in the cell wall, exhibits high levels of immunogenicity<sup>19</sup>. In vitro investigations have corroborated its ability to initiate a CD4<sup>+</sup>T cell response in tuberculosis patients<sup>22</sup>, with extracellular secretion resulting in the presence of 19-KD antigen-specific antibodies in patient serum<sup>23</sup>. Examination of the C-terminus of the 19-KD antigen signal peptide unveils a conserved region (L, S, G), critical for recognition by the Sec secretion pathway signal peptidase II<sup>24</sup>. Following cleavage by this enzyme, the exposed non-polar amino acids L and S may contribute to a spatial configuration reminiscent of  $\beta$ -barrel proteins in the cell wall, facilitating the formation of a channel for the localization of mature proteins<sup>24</sup>. We hypothesize that the mature peptide acts as an anchor to the cell wall.

The 19-KD antigen promoter and signal peptide sequence were integrated into the *Mycobacterium-E. coli* shuttle vector pMV261, yielding the rBCG::RBD strain expressing the wild-type SARS-CoV-2 RBD fused to a mature signal peptide of the 19-KD antigen, named CW-rBCG::RBD (Fig. 1a). Like the previous studies<sup>25–27</sup>, the subcellular fractions were isolated by Triton X-114 (Supplementary Fig. S1a). Lipoprotein isolation from the *M. tb* bacterial lysate was facilitated using Triton X-114. Centrifugation of the lysates yielded a Triton X-114 insoluble fraction enriched with cell wall components and a Triton X-114 detergent-soluble phase containing cell membrane materials<sup>27</sup>. The supernatant obtained from cell lysates was separated into Triton X-114 amphoteric and detergent phases (designated as the cell membrane fraction) and an aqueous phase (designated as the cytoplasm). In this study, Triton X-114 extraction was performed four times on the precipitate obtained by centrifugation of the cell lysate. Both the detergent and aqueous phases were found to contain the RBD antigen, which was identified as the cell membrane being associated with the cell wall. A schematic of the separation process is presented in Supplementary Fig. S1.

In a comparative analysis with control BCG strains harboring an empty pMV261 vector, CW-rBCG::RBD exhibited significantly higher RBD expression, particularly enriched in the cell wall, as confirmed by Western blot analysis, with consistent bacterial quantities ensuring reliable separation. The comparison was made using equivalent optical densities, with equal volumes of cell membrane, cell wall, and cytoplasmic fractions. Heat shock protein 65 (Hsp65), a well-characterized mycobacterial protein, served as the internal control for protein detection (Fig. 1b). Detailed volumes used in subcellular component isolation are presented in Supplementary Fig. S1a. The RBD antigen contained in the cell wall and cell membrane are quantified by the western blot analysis, with integrated density values calculated via ImageJ software. Based on a standard curve generated with known concentrations of RBD-His protein, the RBD antigen contained in the cell wall, following electrophoresis, was determined to be 48.63 ng per 10  $\mu$ l. Considering the volume ratio between the electrophoresis sample and the total cell wall component obtained from final separation (1:180), the total RBD antigen in the cell wall sample was calculated to be approximately 8,753.4 ng. With a volume ratio of whole cell lysate to cell wall component of 7:1 and a total bacterial culture of 72 OD<sub>600</sub> (optical density 600nm), approximately 10.28 OD<sub>600</sub>

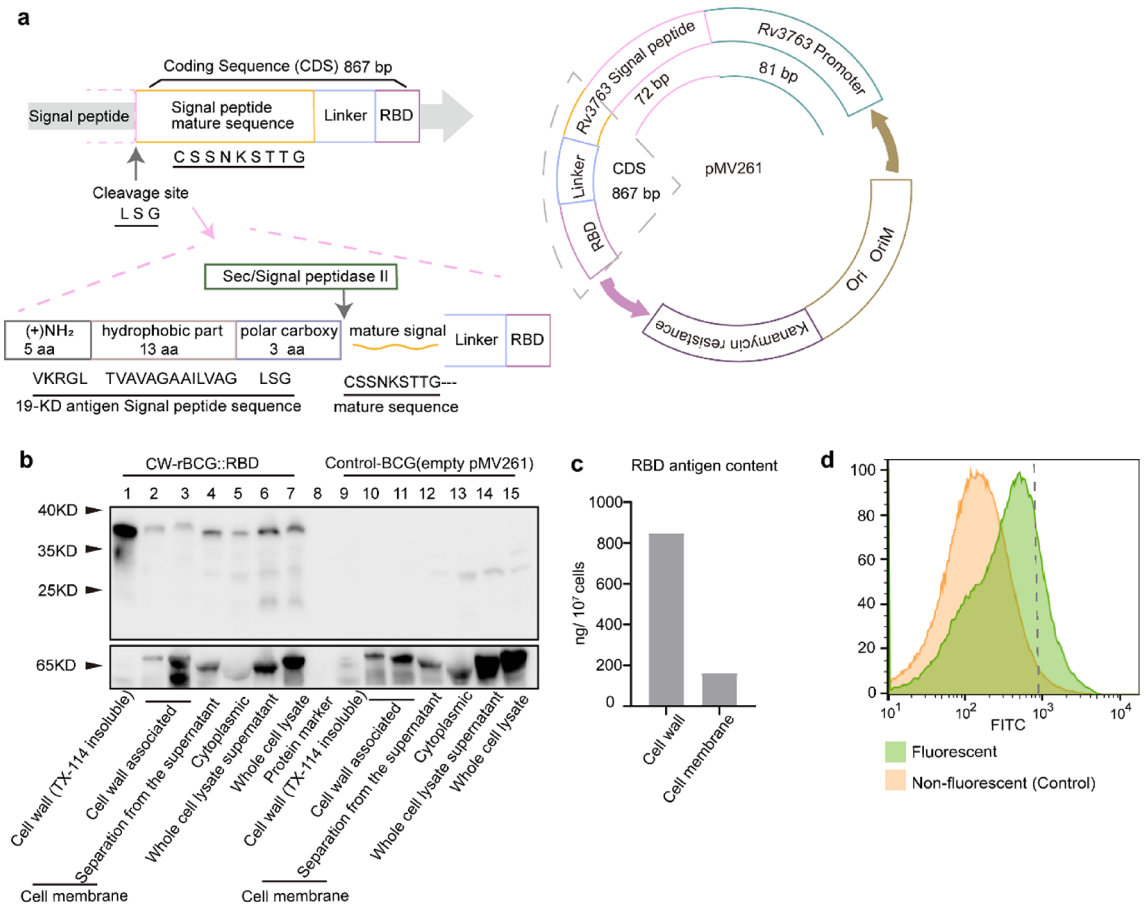


**Fig. 1.** Generation and verification of recombinant BCG strain CW-rBCG::RBD. **(a)** Schematic representation of the coding sequence within the recombinant pMV261 plasmid, encompassing the 19-KD antigen (coding gene *Rv3763*) promoter and signal peptide, linker sequence, and the wild-type SARS-CoV-2 RBD sequence. Illustration depicting the engineering process of the RBD antigen expressed by CW-rBCG::RBD, wherein the signal peptide of 19-KD antigen undergoes cleavage by Sec/signal peptidase II at the preferred restriction site LSG, forming a mature signal peptide with the mature sequence CSSNKSTTG. The mature signal peptide, together with the RBD protein, constitutes the fusion protein expressed by CW-rBCG::RBD. **(b)** Western blot analysis of CW-rBCG::RBD strain to assess the presence of the RBD antigen in subcellular fractions. The RBD antigen band was observed at approximately 35–40 kDa. A negative control was established using the parent BCG Danish strain harboring an empty pMV261 vector. The subcellular constituents of the CW-rBCG::RBD are organized within the identical lanes as those observed in the control group situated on the right-hand side. Subcellular fractions were analyzed in lanes corresponding to the cell membrane and other components: lane 2 represents the Triton X-114 soluble detergent phase extracted from the precipitate; lane 3 represents the Triton X-114 aqueous phase extracted from the precipitate; lane 4 represents the Triton X-114 detergent and amphoteric phases extracted from the supernatant of cell lysate. **(c)** Quantification of RBD antigen content in the cell wall and membrane of CW-rBCG::RBD per  $10^7$  cfu. Integrated density values of the bands were determined via western blot experiments and quantified against RBD-His protein standards using ImageJ software. Details regarding the calculation of CW-rBCG::RBD or BCG quantities used for subcellular component separation, along with corresponding volume ratios, are provided in the Methods, Supplementary Data, and Supplementary Fig. S1b–e. The RBD antigen content in the samples was calculated by estimating the final volume ratios of different subcellular components relative to the total bacterial solution volume during the separation process (Supplementary Fig. S1). **(d)** Flow cytometry confirmed surface expression of RBD on CW-rBCG::RBD. Shown is one representative result from three independent experiments (Supplementary Fig. S1g). Green histogram: stained with anti-RBD antibody and FITC-conjugated secondary antibody. Yellow histogram: shown background fluorescence, anti-RBD antibody only (control).

of CW-rBCG::RBD was found to contain 8,753.4 ng of RBD antigen. Given that an  $OD_{600}$  of 1.0 corresponds to approximately  $10^7$  colony-forming units (cfu), the RBD antigen content in  $10^7$  cfu of CW-rBCG::RBD was estimated at 850 ng. The RBD antigen content in the cell membrane was calculated using the same method as for the cell wall. Detailed analyses of the cell wall and cell membrane fractions are provided in **Supplementary Data 1c, d and Supplementary Fig. S1b–e**. Our results revealed approximately 850 ng of the RBD antigen in the cell wall fraction per  $10^7$  cfu, 163 ng in the cell membrane fraction, and a minor fraction in the cytoplasm, which

was not quantified (Fig. 1c, Supplementary Fig. S1e). To further confirm the surface localization of the RBD on CW-rBCG::RBD, flow cytometry analysis was conducted (Fig. 1d). The CW-rBCG::RBD strain exhibited increased surface fluorescence when treated with an anti-RBD polyclonal antibody followed by a fluorescein isothiocyanate (FITC)-conjugated secondary antibody, compared to the control group treated without the FITC-conjugated secondary antibody. These findings, along with the results from Triton X-114 phase partitioning and subsequent western blot analysis, confirm that the 19-kD antigen signal peptide and promoter effectively facilitated the expression of the 19-kD antigen mature signal peptide-RBD fusion protein, with significant enrichment in the Triton X-114 insoluble (cell wall) fraction. Notably, no secreted 19-kD antigen mature signal peptide-RBD fusion protein was observed in the cell culture (Supplementary Fig. S1f), indicating that the 19-kD antigen signal peptide and promoter enable abundant antigen display on the cell wall.

### CW-rBCG::RBD induced antigen-specific neutralizing antibodies in mice

To evaluate whether recombinant BCG (rBCG) strain can elicit antibodies responses after immunization, CW-rBCG::RBD was tested in BALB/c mice using a single intravenous dose ( $10^6$  or  $10^5$  cfu) and a prime-boost regimen with a booster ( $10^6$  cfu) at 4 weeks. Control groups received PBS, parent BCG ( $10^6$  cfu), or the RBD protein subunit vaccine (RBD<sup>AS01</sup>), which contains 10 µg RBD-His recombinant protein adjuvanted with 5 µg AS01, a liposome-based adjuvant designed for rapid humoral responses<sup>28</sup>(Fig. 2a).

As shown in Fig. 2b, at 4- and 8 weeks post-immunization, RBD-specific IgG and Nab titers were measured. A single intravenous dose of  $10^6$  cfu CW-rBCG::RBD elicited a detectable IgG titer of 1,600, whereas the same dose of parent BCG,  $10^5$  cfu CW-rBCG::RBD or subcutaneous administration of CW-rBCG::RBD at the same dose failed to generate significant RBD-specific IgG responses. In Fig. 2c, the two-dose prime-boost regimen resulted in a further increase in RBD-specific IgG titers to 3,200 by week eight, whereas the titers in the BCG comparison group remained below 400 (Fig. 2c). Importantly, RBD Nab titers in CW-rBCG::RBD-immunized mice reached 4,485, significantly higher than the modest Nab levels in mice immunized with parent BCG (160), RBD<sup>AS01</sup>(5.109) (Fig. 2d). These findings demonstrate that intravenous administration of CW-rBCG::RBD effectively induces strong humoral responses, including RBD-specific IgG and Nabs, with enhanced potency compared to other immunization strategies or control groups. The presence of the RBD antigen on the BCG cell wall may play a critical role in driving this immune response.

### CW-rBCG::RBD induced antigen-specific cellular responses in mice

Recombinant BCG strains expressing homologous antigens have been shown to elicit T helper (Th) cell responses<sup>7</sup>, however, the role of cell wall-associated antigens in these responses is less understood. Since Tfh cells are crucial for germinal center (GC) formation and antibody production<sup>29</sup>, we hypothesized that CW-rBCG::RBD would also enhance Tfh cell frequency. To test this, we evaluated the RBD-specific cellular immune responses in mice 12 weeks after intravenous immunization, a timepoint that reflects long-term memory responses. We compared the results to parent BCG and an RBD protein subunit vaccine (RBD<sup>AS01</sup>), all of which were boosted at week 2. The same dose of parental BCG served as a control to gauge the RBD-specific response.

At the 12-week endpoint, spleens from CW-rBCG::RBD-immunized mice showed significantly increased Tfh cell activation compared to both parent BCG and RBD<sup>AS01</sup> groups (Fig. 3b). Tfh cells were identified in the spleen by flow cytometry as CD4<sup>+</sup>CD44<sup>+</sup> CD62L<sup>-</sup> cells co-expressing the Tfh signature markers CXCR5 and PD-1, along with the germinal center marker GL7. This suggests that CW-rBCG::RBD elicited sustained Tfh cell activation and expansion of antigen-specific Tfh cells. In contrast, the RBD<sup>AS01</sup> vaccine alone failed to induce significant Tfh responses when compared to PBS controls, highlighting the role of CW-rBCG::RBD in driving Tfh cell activation.

In addition to Tfh cells, Tcm cells, which are important for long-term immunity<sup>30</sup>, were significantly elevated in the spleens of CW-rBCG::RBD prime-boosted mice compared to both parent BCG and RBD<sup>AS01</sup> groups at week 12 (Fig. 3c). Notably, the RBD<sup>AS01</sup> vaccine alone group elicited Tcm cell frequencies comparable to those of the PBS control, indicating limited memory induction. In contrast, mice immunized with a single dose of CW-rBCG::RBD exhibited a markedly stronger Tcm response than those receiving parental BCG (Fig. 3d). ELISPOT assays further confirmed a significant increase in the number of cells secreting IFN-γ, a hallmark of memory T cell responses, in the CW-rBCG::RBD group (Fig. 3e). These results suggest that CW-rBCG::RBD induces strong memory T cell responses, even with a single dose.

### Priming with CW-rBCG::RBD elicits strong early neutralizing antibodies, Th1-IgG2a bias, and durable RBD-specific CD8<sup>+</sup> T cell responses

Given the essential role of Tfh cells in promoting high-quality antibody responses, we hypothesized that priming with CW-rBCG::RBD followed by boosting with the RBD<sup>AS01</sup> would enhance humoral immunity compared to the RBD<sup>AS01</sup>-alone regimen. To test this, we evaluated Nabs titers at 8 and 16 weeks following intravenous immunization with CW-rBCG::RBD, BCG-primed RBD<sup>AS01</sup>, or RBD<sup>AS01</sup> alone (Fig. 4a).

At 8 weeks, the CW-rBCG::RBD primed group exhibited significantly higher RBD-specific Nab titers (10,321) compared to the BCG priming group (4,803) and the RBD<sup>AS01</sup>-alone group (1,174) (Fig. 4b). The Nab titers in the RBD<sup>AS01</sup>-alone group were much lower, likely due to the absence of the Tfh cell activation induced by CW-rBCG::RBD. By 16 weeks, Nab titers decreased across all groups, but both CW-rBCG::RBD and BCG-primed groups maintained significantly higher titers (2,375 and 2,802, respectively) compared to the RBD<sup>AS01</sup>-alone group (759.5) (Fig. 4c). This decline may be partially attributed to antigen clearance following intravenous immunization, as discussed in the manuscript, suggesting that single-dose intravenous recombinant BCG primarily induces a T cell-dominated response rather than sustained humoral immunity.

To further explore this, we evaluated cytokine secretion in response to antigenic stimulation. T cells isolated from the spleens and lungs of immunized mice were restimulated with an RBD peptide pool. At both 8 and 12

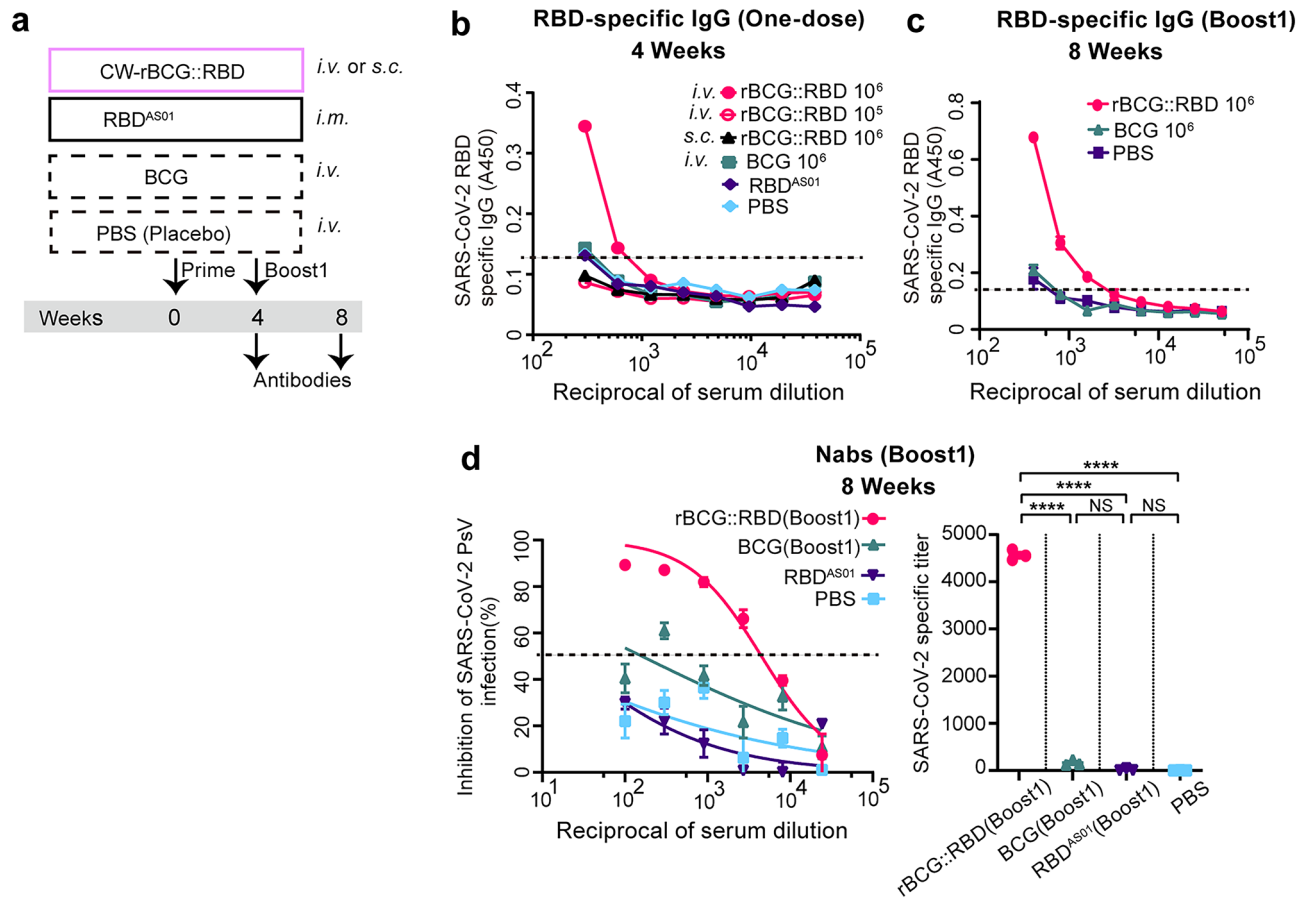


**Fig. 2.** Intravenous immunization with CW-rBCG::RBD rapidly induces anti-RBD Nabs responses in mice. **(a)** Schematic overview of the immunization protocols, including the timeline and grouping for vaccination and monitoring of antibody responses across four groups of vaccinated mice. Eight-week-old BALB/c mice were immunized with indicated dose and route of CW-rBCG::RBD at week 0, or followed by a booster at week 4. Blood samples were collected at week 4 and 8 to evaluate RBD-specific IgG titers and neutralizing titers, respectively. **(b-c)** ELISA analysis of RBD-specific IgG titers in pooled sera from each group at weeks 4 **(b)** and 8 **(c)**. CW-rBCG::RBD groups are labeled as “rBCG::RBD” with “10<sup>6</sup>” indicating the standard-dose group (10<sup>6</sup> cfu/ml) and “10<sup>5</sup>” representing a 10-fold lower dose. Mice were immunized intravenously (*i.v.*), subcutaneously (*s.c.*), or intramuscularly (*i.m.*) as specified. Prime denotes the initial immunization, while Boost1 refers to the first booster dose. RBD-specific IgG titers were defined as the serum dilution factor at which the absorbance at 450 nm was twice the value of the maximum dilution from PBS-immunized controls. The dotted line represents the detection limit. All experiments were performed at least twice, with data presented as the geometric mean  $\pm$  SEM from two independent experiments, using six mice per group in each. **(d)** Neutralizing antibody titers (NT<sub>50</sub>) values at week 8 post-immunization were measured using a SARS-CoV-2 RBD pseudovirus (PsV) neutralization assay. Sera from six mice per group were pooled in equal volumes. Data are presented as geometric mean  $\pm$  SEM from two independent experiments (with two replicates in experiment 1). The right panel shows percent inhibition curves used to calculate NT<sub>50</sub> values (50% inhibition of PsV infection), analyzed by non-linear regression in GraphPad Prism. Statistical significance was assessed by an one-way ANOVA. Statistical significance is indicated as \*\*\*\**p* < 0.0001.

weeks post-immunization, the CW-rBCG::RBD-primed group followed by RBD<sup>AS01</sup> boosting showed a high frequency of IFN- $\gamma$ -secreting CD8<sup>+</sup> T cells (**Fig. 4d, e**). Notably, at 12 weeks, mice in the BCG-primed group exhibited increased IFN- $\gamma$ -producing CD4<sup>+</sup> T cells in the lungs (**Fig. 4e**), suggesting enhanced Th cell activation and a Th1-skewed immune profile, consistent with the known adjuvant properties of BCG<sup>10,31,32</sup>.

T cells from mice receiving CW-rBCG::RBD priming followed by RBD<sup>AS01</sup> boosting secreted substantial amounts of IFN- $\gamma$  in response to RBD peptide stimulation (**Fig. 4f**), indicating durable antigen-specific cellular immunity. These findings support the notion that surface-displayed antigens on recombinant BCG effectively stimulate CD8<sup>+</sup> T cell responses, contributing to enhanced antiviral defense.

Studies have linked Th1 responses to the production of IgG2a isotype antibodies, indicative of a Th1 bias<sup>29,31,33</sup>. Murine IgG2a closely resembles human IgG1 in pharmacokinetics and Fc effector function, making it a common surrogate in preclinical studies<sup>34</sup>. To further investigate the effect of CW-rBCG::RBD on IgG subclass production, we assessed RBD-specific IgG subtypes following priming with CW-rBCG::RBD and boosting with

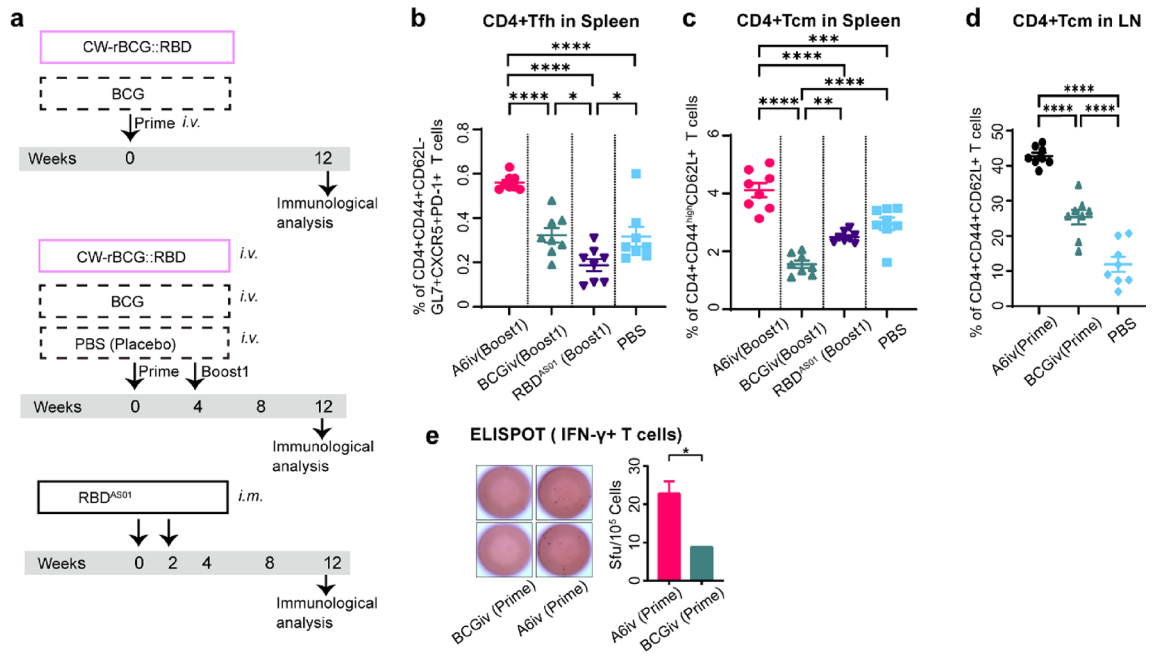


**Fig. 3.** The RBD-specific cellular immune responses elicited by the CW-rBCG::RBD compared with BCG and RBD<sup>AS01</sup>. Single-cell suspensions from spleens, inguinal lymph nodes, and lungs were pooled from six mice per group and divided into four replicates for assays at week 12. Cells were restimulated ex vivo with 2.5 μg/ml SARS-CoV-2 RBD peptide pool for 44 h, followed by flow cytometry to assess Tfh and Tcm responses. **(a)** Immunization schedule and experimental grouping. **(b)** Detection of Tfh cells (CD4<sup>+</sup>CD44<sup>+</sup>CD62L<sup>-</sup>GL7<sup>+</sup>CXCR5<sup>+</sup>PD-1<sup>+</sup>) in boosted mice. Gating strategy and representative plots shown in Supplementary Fig. S5a–b. **(c)** CD4<sup>+</sup>Tcm (CD4<sup>+</sup>CD44<sup>+</sup>CD62L<sup>-</sup>) detection in the boosted group and **(d)** primed group; gating shown in Supplementary Fig. S4c. **(e)** IFN-γ-secreting cells per 10<sup>5</sup> lung cells measured by ELISPOT. Two wells represent data from two independent experiments, statistical analysis was performed using a *t*-test. In (b)–(d), data are from two independent experiments, each with four replicates. Data are presented as mean ± SEM. Statistical analysis was performed using an one-way ANOVA, with significance indicated as \**p* < 0.05, \*\**p* < 0.01, \*\*\**p* < 0.001, \*\*\*\**p* < 0.0001.

a single-dose RBD<sup>AS01</sup>. Two weeks post-priming, the CW-rBCG::RBD priming group showed the highest RBD-specific IgG titers (10,240), approximately 16-fold higher than the BCG-primed group (640). In comparison, RBD<sup>AS01</sup> alone generated minimal IgG responses (320) (**Fig. 4g**). Notably, CW-rBCG::RBD priming significantly increased RBD-specific IgG2a production, with the titer is 4,860, whereas BCG priming elicited negligible IgG2a responses (**Fig. 4h**). When BCG priming followed by RBD<sup>AS01</sup> boosting, the response was predominantly IgG1, with titers of 180 in the BCG-primed group and 1,620 in the CW-rBCG::RBD-primed group (**Fig. 4i**). The IgG2a-to-IgG1 ratio in the CW-rBCG::RBD group was 3, reflecting a strong Th1 bias (**Fig. 4j**), which is critical for the generation of an effective immune response against viruses<sup>35,36</sup>. Additionally, at week 12, bone marrow B cell responses were assessed, revealing increased proportion of in IgG2a<sup>+</sup> RBD<sup>+</sup> B cells in the CW-rBCG::RBD group (**Fig. 4k**). These results underscore the ability of CW-rBCG::RBD to promote long-lasting IgG2a<sup>+</sup> RBD<sup>+</sup> B cell responses, which are essential for sustained immunity.

Together, these findings confirm that CW-rBCG::RBD induces a robust, Th1-skewed immune response, characterized by elevated IgG2a antibody production and enhanced IgG2a<sup>+</sup> RBD<sup>+</sup> B cell responses. In contrast, parent BCG primarily acts as an adjuvant, eliciting a more generalized immune response with lower RBD-specific antibody production. Additionally, intravenous BCG immunization has been shown to protect against lethal SARS-CoV-2 challenge<sup>37</sup>, suggesting that CW-rBCG::RBD, when administered intravenously, has the potential to provide protection against viral infections. The durable RBD-specific T cell responses observed in the CW-rBCG::RBD group further support the advantages of this vaccine platform in enhancing immune responses for long-term protection.

### Subcutaneous administration of CW-rBCG::RBD enhances long-term humoral immunity

The effectiveness of rBCG in inducing cellular immune responses is influenced by the route of administration (e.g., intravenous vs. subcutaneous)<sup>38</sup>. In **Fig. 2a**, subcutaneous immunization with CW-rBCG::RBD alone failed to induce RBD-specific antibody production, and co-administration with a single dose of RBD<sup>AS01</sup> also did not generate RBD-specific antibodies (Supplementary Fig. S3). However, recent investigations suggest that co-administration of parent BCG with protein vaccines can enhance antigen-specific humoral responses<sup>10</sup>. In our experiments, subcutaneous co-administration of CW-rBCG::RBD with the RBD<sup>AS01</sup> (administered intramuscularly) (**Fig. 5a**), significantly improved humoral responses, sustaining Nab titers at high levels. At week 16, the Nabs titers were quantified at 5,635 for the CW-rBCG::RBD co-administration group, 1,909 for the

BCG co-administration group, and 1,778 for the RBD<sup>AS01</sup>-alone group (Fig. 5b). Notably, BCG co-administration with RBD<sup>AS01</sup> did not significantly enhance RBD-specific Nabs production at week 16 ( $p > 0.05$ ), whereas CW-rBCG::RBD co-administration markedly increased Nabs production ( $p < 0.01$ ).

Longitudinal analysis of Nab titers at week 31 revealed endpoint Nabs titers of 1,795 for the CW-rBCG::RBD co-administration group, 414.5 for the BCG co-administration group, and 0.7 for the RBD<sup>AS01</sup>-alone group (Fig. 5c). The CW-rBCG::RBD group demonstrated significantly higher titers compared to the BCG co-administration group ( $p < 0.001$ ) and the RBD<sup>AS01</sup>-alone group ( $p < 0.001$ ), highlighting its ability to sustain RBD-specific Nab responses over time.

Consistent with the antibody responses, analysis of spleen samples from mice immunized for 12 weeks showed a significantly higher ratio of CD4<sup>+</sup> Tfh cells in the CW-rBCG::RBD co-administration group compared to the BCG co-administration group, which was similar to PBS (Fig. 5d). In addition, in the lungs, Tcm cell frequency was markedly higher in the CW-rBCG::RBD co-administration group, while nearly absent in the BCG and RBD<sup>AS01</sup>-alone groups, both resembling the PBS group (Fig. 5e). These findings suggest that CW-rBCG::RBD co-administration elicited stronger Tfh and Tcm cell responses, particularly in the presence of RBD peptide pool stimulation *ex vivo*, indicating enhanced RBD-specific memory T cell responses. In summary, the combined immunization of CW-rBCG::RBD with protein subunit vaccines, results in an enhancement of RBD-specific T cell responses, outperforming BCG co-administration, which primarily elicits non-specific T cell responses. These results suggest that subcutaneous immunization may be a preferable route for eliciting long-lasting antibody-mediated immunity.

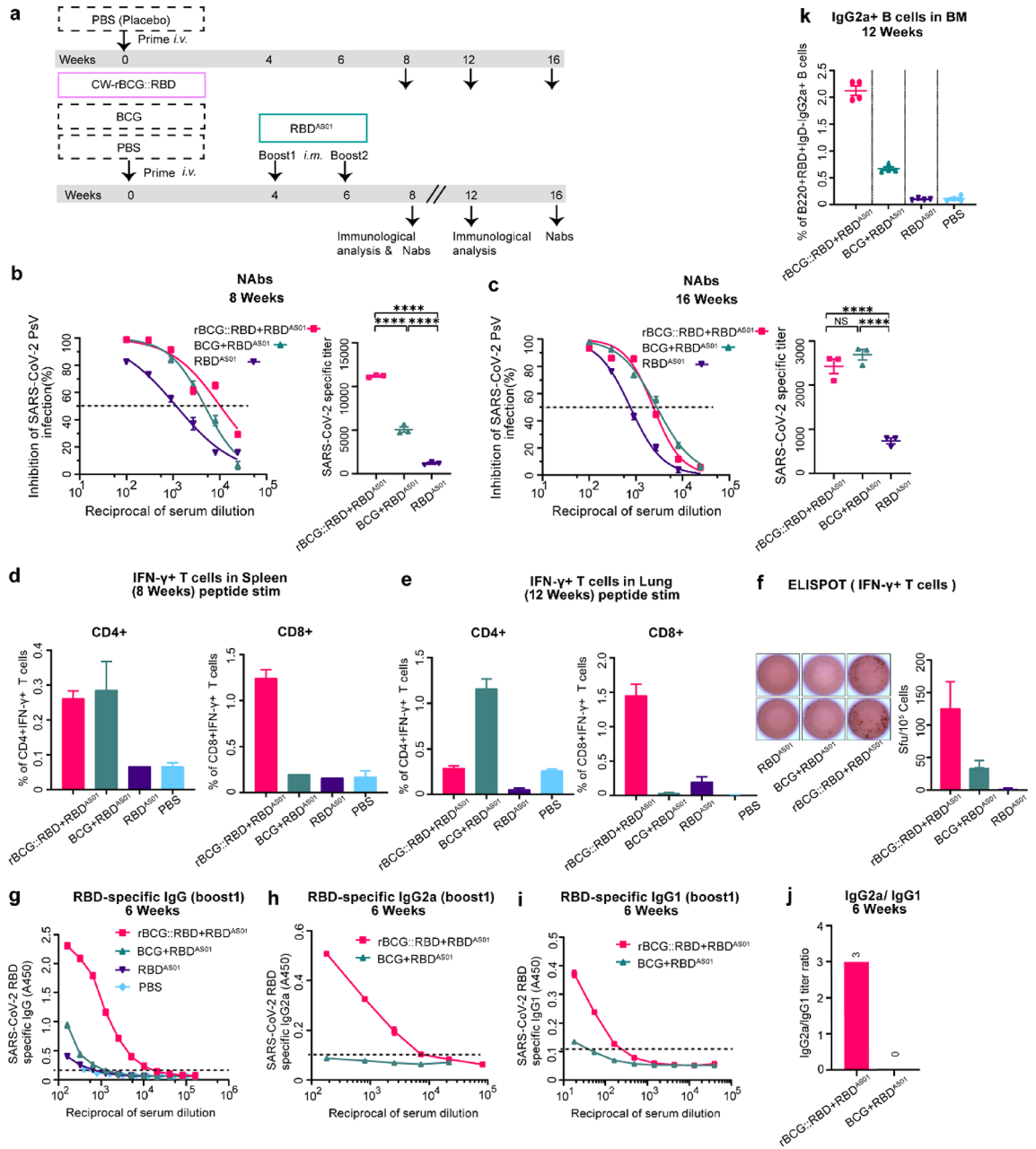
## Discussion

The administration of BCG is widely recognized for its established safety profile across all age groups, making it an attractive candidate for antigen delivery. As a live vaccine, BCG can replicate within the host and thereby induce prolonged immune responses. Additionally, it possesses inherent adjuvant properties that enhance immune responses to delivered antigens, potentially leading to long-lasting protection against pathogens. In addition, researchers have explored the potential of rBCG as a vector for delivering tumor-associated antigens and enhancing the immune response against cancer cells<sup>1,2,39</sup>. By combining BCG's ability to stimulate innate immunity with genetic modifications to express tumor-specific antigens, rBCG offers a promising platform for cancer treatment. However, challenges remain, including the tumor's immune evasion mechanisms and the need for optimizing the delivery routes of rBCG for maximum therapeutic efficacy.

In contrast to its role in anti-tumor immunity, protection from infection can be achieved by eliciting Nabs<sup>40,41</sup>, through the induction of Tfh cell responses in GCs<sup>11</sup>. Thus, identification of vaccine platforms that strongly promote Tfh cell and GC responses is critical for developing effective humoral immunity against emerging infections. However, how to construct rBCG to elicit heterologous antigen-specific Nab responses remains unclear. Our results found that CW-rBCG::RBD immunized intravenously elicited the Tfh cellular responses and this effect could be maintained at 12 weeks post-vaccination, which indicated the long-term cellular responses. While in previous rBCG studies, antigen-specific Tfh cell responses and robust humoral responses were not observed. This suggests that CW-rBCG::RBD may enhance Nab production through Tfh cell activation. Notably, durable Tfh cellular activation could compensate for the limited long-term cellular immune responses and antibody production that protein vaccines alone cannot elicit.

Several rBCGs have been studied for antiviral vaccine development over the years, providing immune protection but often lacking the ability to elicit Nabs<sup>3-7,14</sup>. Such protection may be partially attributed to BCG's capacity to induce non-specific cellular immune responses, commonly referred to as trained immunity. Supporting this, recent studies have shown that intravenous BCG immunization can significantly reduce viral loads in the lungs of rhesus macaques<sup>42</sup> and confer protection against SARS-CoV-2 challenge in mice<sup>37</sup>. In our study, intravenous BCG similarly induced non-specific cellular responses (Fig. 3b-d) and strong anti-BCG IgG production (Supplementary Fig. S2), although the functional role of these BCG-elicited antibodies remains poorly understood. Emerging evidence suggests that BCG or related mycobacterial exposure can elicit heterologous antibody isotypes, including IgM<sup>43</sup>. Consistently, our data (Fig. 2d) show minimal neutralizing antibody responses following intravenous BCG immunization, which may be insufficient to confer biologically meaningful protection. We further speculate that pre-existing anti-BCG antibodies generated after a single 10<sup>6</sup> cfu BCG (*i.v.*) dose may impair BCG persistence by promoting its clearance from host tissues. Indeed, previous studies have demonstrated that BCG (*i.v.*) is rapidly eliminated: in mice administered 10<sup>6</sup> cfu, only ~10<sup>4</sup> cfu remained in the lungs three days post-immunization—a 100-fold reduction<sup>37</sup>. Similarly, in rhesus macaques receiving 5 × 10<sup>5</sup> cfu BCG (*i.v.*), cfus in the skin and lymphoid tissues declined by ~10<sup>4</sup>-fold within one month<sup>43</sup>, indicating limited systemic antigen persistence.

The limited ability of rBCG candidates to induce Nabs may be attributed to subcellular antigen localization. Most previous constructs expressed antigens intracellularly, where processing is predominantly restricted to MHC class II pathways, limiting their ability to induce robust humoral responses, potentially reducing effective antigen presentation and immune activation. In contrast, our RBD-displaying rBCG may facilitate enhanced antigen uptake and cross-presentation via MHC class I, thereby promoting CD8<sup>+</sup> T cell priming. This was supported by the strong CD8<sup>+</sup> T cell responses observed following RBD<sup>AS01</sup> boosting, which were absent in the wild-type BCG group, where the response was primarily CD4<sup>+</sup>-driven (Fig. 4d-e). This highlights the adjuvant-like role of BCG (*i.v.*). Additionally, many previous rBCG designs lacked signal peptides for cell wall localization, further limiting immune activation. Due to the variations in antigen type, dose, and delivery route across studies, along with underreporting of critical parameters such as Tfh induction, memory T cells, and antigen localization, it is difficult to directly compare the results with our findings and underscore the need for improved design strategies<sup>3-7</sup>. These gaps highlight the need for continued development of rBCG strategies, particularly focusing on cell wall antigen localization. Presenting antigens on the cell wall appears to enhance immunogenicity by



facilitating early interaction with host immune cells, potentially improving the vaccine’s ability to elicit robust immune responses. In our study, we developed an rBCG displaying the RBD on the cell wall, showing that this approach elicits T<sub>h</sub> cell responses and enhances RBD-specific cellular and humoral immunity, especially when combined with an RBD protein subunit vaccine to induce durable Nabs. Additionally, we found that both intravenous and subcutaneous administration of CW-rBCG::RBD could elicit T<sub>h</sub> cell responses and prolong the duration of Nab production when combined with the RBD protein subunit vaccine. This approach provides a promising strategy for improving rBCG’s ability to elicit Nabs.

Various lipoprotein signal peptides and promoters were tested for their ability to facilitate high-level expression of recombinant antigens on the rBCG cell wall. However, not all were effective, likely due to differences in promoter activity and the plasmid vector, with the signal peptide being the primary influencing factor. For instance, the PPE25 signal peptide, derived from the PPE family of *Mycobacterium tuberculosis*, known for eliciting humoral responses, showed reduced RBD antigen localization to the cell wall and weaker immune responses compared to CW-rBCG::RBD. Specifically, the PPE25-rBCG::RBD vector elicited only minimal RBD-specific IgG responses (titer of 640), and Nabs were undetectable using the pseudovirus neutralization test. Moreover, co-immunization with RBD<sup>AS01</sup> did not enhance IFN- $\gamma$ -secreting T cell responses, similar to the parent BCG group, as demonstrated by ELISPOT and flow cytometry analyses (**unpublished data, Supplementary Fig. S6**). Interestingly, the PPE25-rBCG::RBD vector constructed using the pMV306 plasmid expressed the RBD antigen, whereas the pMV261-based vector with the same elements failed to do so. These findings highlight the superiority of CW-rBCG::RBD in driving robust and long-lasting immune responses.

◀ **Fig. 4.** Intravenous vaccination of CW-rBCG::RBD followed by RBD<sup>AS01</sup> enhances Nabs production and induces Th1-biased cellular responses along with IgG2a subtype antibody generation. **(a)** Schematic overview of the immunization protocols. BALB/c mice were intravenously vaccinated with PBS, BCG, or CW-rBCG::RBD, followed by two doses of RBD<sup>AS01</sup> at week 4 and 6. Whole blood was collected at week 6 after the first boost with RBD<sup>AS01</sup>, at week 8 and 16 to assess Nabs. **(b, c)** Neutralizing antibody titers (NT<sub>50</sub>) values at 8 weeks **(b)** and 12 weeks **(c)** post-immunization were determined using pooled sera in the SARS-CoV-2 RBD PsV neutralization assay. Sera from six mice per group were pooled in equal volumes. Data are presented as geometric mean ± SEM from two independent experiments (with two technical replicates in experiment 1). **(d-f)** Splens and lungs from each group of six mice were pooled and divided into four aliquots for downstream assays. Single-cell suspensions from spleens (collected at 8 weeks) and lungs (at 12 weeks) were restimulated *ex vivo* with 2.5 µg/ml of a SARS-CoV-2 RBD peptide pool for 44 h. IFN-γ production by CD4<sup>+</sup>T cells **(d)** and CD8<sup>+</sup>T cells **(e)** was assessed by intracellular cytokine staining and analyzed via flow cytometry. The gating strategy is shown in Supplementary Fig. S4. Data are presented as geometric mean ± SEM from a single experiment. **(f)** ELISPOT assay quantifying the number of IFN-γ secreting cells per 10<sup>5</sup> lung cells, each well represents a replicate of the experimental sample. Data are presented as geometric mean ± SEM. **(g-i)** RBD-specific IgG **(g)**, IgG2a **(h)**, and IgG1 **(i)** titers in sera pooled from each group were measured by ELISA. Boost 1 refers to the administration of a single dose of RBD<sup>AS01</sup> following the priming immunization. Titers were defined as the serum dilution factor at which absorbance at 450 nm was twice the value of the maximum dilution of PBS-immunized controls. The dotted line represents the detection limit. All experiments were performed at least twice. **(j)** The IgG2a to IgG1 ratio for all groups. **(k)** Bone marrow samples were collected at week 12, pooled from six mice per group, and analyzed in four replicates from a single experiment. Flow cytometry was performed to identify IgG2a<sup>+</sup> B cells (B220<sup>+</sup> IgD<sup>-</sup> IgG2a<sup>+</sup> RBD<sup>+</sup>). Data are presented as geometric mean ± SEM from four replicates of a representative experiment. In **(b)**- **(c)**, statistical analysis was performed using an one-way ANOVA, with significance indicated as \*\*\*\**p* < 0.0001.

Our data show that intravenous immunization with CW-rBCG::RBD in a prime-boost regimen elicited RBD-specific Nabs, along with significantly higher Tfh cell frequencies compared to the BCG control (Fig. 3). Tfh cells are essential for supporting B cell differentiation and antibody production, suggesting that the surface-displayed RBD antigen on BCG was effectively recognized by antigen-presenting cells (APCs). This efficient antigen processing likely contributed to robust T cell activation. Notably, B cells, which can function as both APCs and antibody producers, may have played a dual role by recognizing the RBD antigen on the rBCG surface and subsequently secreting RBD-specific antibodies. However, intravenous immunization also induced BCG-specific antibody production, which may have constrained the increase in RBD-specific titers (Supplementary Fig. S2). This observation explains why CW-rBCG::RBD (*i.v.*) alone did not generate higher Nab titers. Additionally, experiments with lower intravenous doses of CW-rBCG::RBD, combined with RBD<sup>AS01</sup>, revealed distinct immune profiles (Supplementary Fig. S4b-f). For instance, a single low-dose intravenous immunization (10-fold lower than the standard dose) followed by boosting with RBD<sup>AS01</sup> elicited higher Tcm responses at 8 weeks post-immunization compared to the standard-dose group (Supplementary Fig. S4f). However, by week 12 post-immunization, the standard-dose group elicited the highest Tcm responses (Supplementary Fig. S4e). Similarly, the prime-boost regimen resulted in lower Tcm responses compared to single-dose immunization in lymph nodes (Supplementary Fig. S4d), emphasizing that vaccine dosage significantly influences immune outcomes. Despite the potent immune responses observed, intravenous administration poses practical and safety challenges in clinical settings, necessitating further optimization for potential use. Co-administration of CW-rBCG::RBD with RBD<sup>AS01</sup> via the subcutaneous route induced durable Nabs by 31 weeks postimmunization, underscoring the importance of optimizing key parameters such as the vaccination route, subunit vaccine dose and booster timing to maximize efficacy. Future studies should evaluate the protective efficacy of CW-rBCG::RBD against viral infections through challenge experiments and true virus neutralization assays, if feasible. Additionally, the potential for recombinant BCG to induce trained immunity may offer non-specific immune activation, enhancing protection against other pathogens and contributing to pandemic preparedness<sup>44-46</sup>. Overall, our findings demonstrate that CW-rBCG::RBD can serve as a promising vaccine platform, inducing robust and long-lasting immune responses, particularly when combined with a subunit vaccine, and highlighting its potential for future pandemic vaccines.

## Materials and methods

### Bacterial strains and plasmids

BCG (strain Danish) was cultured at 37 °C in Middlebrook 7H9 media (BD, New Jersey, USA) supplemented with 0.5% glycerol, 0.02% Tyloxapol, and 10% albumin-dextrose-catalase, or on solid Middlebrook 7H10 media supplemented with oleic acid-ADC. Single-cell suspensions were prepared from cultures in exponential phase (Optical density 600 nm ranging from 0.8 to 1.0) by washing in PBS, sonication for 30 s, and centrifugation at 3,000 g for 10 min to remove residual bacterial clumps. BCG suspensions were diluted in PBS, and colony-forming units for vaccination were cultured on supplemented Middlebrook 7H10 agar plates.

### Construction of SARS-CoV-2 receptor binding domain (RBD) expression vector

The SARS-CoV-2 RBD antigen, 19-KD antigen (coding gene *Rv3763*) gene promoter region, and RBD gene sequences were PCR-amplified using NEB Q5 High-Fidelity DNA Polymerase. The *Rv3763* promoter region and signal peptide sequence were sourced from *Mycobacterium tuberculosis H37Rv* genomic DNA. The RBD gene (GenBank: PP522461.1), corresponding to amino acids 367–606 of the SARS-CoV-2 spike S1 protein, was

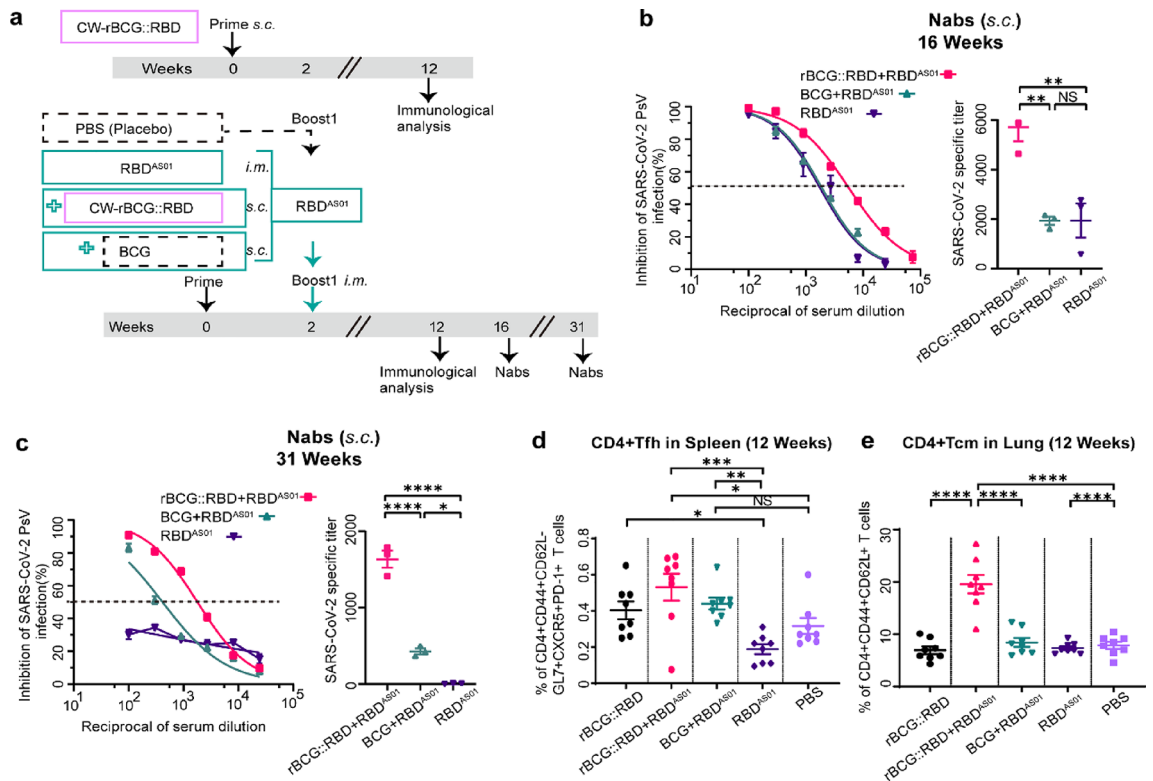


**Fig. 5.** Subcutaneous co-administration of CW-rBCG::RBD with RBD<sup>AS01</sup> enhances neutralizing antibodies and RBD-specific memory T cells. **(a)** Schematic overview of the immunization protocols. BALB/c mice were subcutaneously vaccinated in the footpad with standard-dose BCG, standard-dose CW-rBCG::RBD combined with RBD<sup>AS01</sup> (i.m.), or RBD<sup>AS01</sup> alone (i.m.). All groups received a subsequent boost with RBD<sup>AS01</sup> after 2 weeks. **(b, c)** Neutralizing antibody titers (NT<sub>50</sub>) values were measured via a SARS-CoV-2 RBD PsV neutralization assay at 16 weeks **(b)** and 31 weeks **(c)** using the sera from six mice per group were pooled in equal volumes. Data are presented as geometric mean  $\pm$  SEM from two independent experiments (with two technical replicates in experiment 1) **(d, e)** Memory T cell responses were assessed 12 weeks post-immunization by flow cytometry. Samples from each group were pooled and divided into four aliquots for downstream assays, resulting in four technical replicates per experiment. Splens cells were analyzed for Tfh cells **(d, CD4<sup>+</sup> CD44<sup>+</sup> CD62L<sup>-</sup> GL7<sup>+</sup> CXCR5<sup>+</sup> PD-1<sup>+</sup>)**, and lung cells for Tcm cells **(e, CD4<sup>+</sup> CD44<sup>+</sup> CD62L<sup>+</sup>)** following *ex vivo* restimulated with 2.5  $\mu$ g/ml of SARS-CoV-2 RBD peptide pool. Data were obtained from two independent experiments, each involving 6 mice per group. Data are presented as geometric mean  $\pm$  SEM. Significant differences between groups were determined by one-way ANOVA, with significance indicated as \* $p < 0.05$ , \*\* $p < 0.01$ , \*\*\* $p < 0.001$ , \*\*\*\* $p < 0.0001$ .

amplified from the RBD vector plasmid fused with the linker sequence GGTGGAGGCGGTTTCAGGCGGAG GTGGCTCTGGCGGTGGCGGATCGCAAGCT. Primer sequences were designed for the amplification of the *M. tuberculosis* Rv3763 promoter and the SARS-CoV-2 RBD gene. For amplification of the Rv3763 promoter: Forward primer: GCTCTAGAGGCAGTGGGAGGTTTGTGTTCCATCG. Reverse primer: CGGGATCCT TATCCTGTAGTCGACTTGTGCTTGAACATC. For amplification of the linker sequence and the SARS-CoV-2 RBD gene: Forward primer: GCAACAAGTCGACTACAGGAGGTGGAGGCGGTTTCAGGCG. Reverse primer: CTTCGAATTCTGCAGCTGGATCTTAACCTACGCTCAAGTGTCTGTGGATCAGC. The resulting PCR products were cloned into the *Mycobacterium-E. coli* shuttle vector pMV261 without the *hsp65* promoter using homologous recombination enzyme mix (ToLOBio, China). The recombinant plasmid was validated through DNA sequencing by Qingke Biotech (Shanghai, China).

#### Generation of Recombinant *Mycobacterium bovis* BCG expressing SARS-CoV-2 RBD protein

BCG was transformed by electroporation with either the pMV261-RBD plasmid or the empty vector pMV261. Electroporation was performed using the GenePulser Xcell™ electroporation machine (Bio-Rad, California, USA) at 2.5 kV, 25  $\mu$ F, and 1,000  $\Omega$  conditions. Transformants were then plated and selected on Middlebrook 7H10 agar medium supplemented with 0.5% glycerol and 10% OADC (Becton, New Jersey, USA), containing 50  $\mu$ g/ml kanamycin, for 4 weeks at 37 °C. Colonies were confirmed by PCR using the RBD forward and reverse primers as specified above.

### Characterization and Western blot analysis of RBD antigen in subcellular fractions

The assay followed established protocols<sup>27</sup>. Triton X-114 phase partitioning localized the RBD antigen in recombinant BCG. Cells were harvested, suspended in PBS, and sonicated to yield a whole-cell lysate. Membranes were solubilized with Triton X-114 (2% vol/vol) at 4 °C, resulting in the sedimentation of the cell wall-enriched fraction at 15,000 rpm. Detergent phase partitioning isolated the cell membrane and cytoplasm fraction after centrifugation at 15,000 rpm for 1 h. Protein precipitation with acetone was performed after back-extracting the phases four times. BCG subcellular fractions were reconstituted with 75 mM Tris-buffer. Concentrated culture supernatant underwent SDS-PAGE, PVDF membrane transfer, and blotting with anti-RBD polyclonal antibodies (1:5,000, Biodragon, China). Endogenous Hsp65 was detected with anti-mouse *Mycobacteria* Hsp65 antibody (1:10,000), followed by secondary HRP-conjugated IgG (Sigma, USA). The SARS-CoV-2 RBD-His protein from Easy Biotech (Shanghai, China) served as the protein standard for quantification. Integrated density analysis of electrophoretic bands was performed using ImageJ software. A standard curve was constructed based on the integrated intensities of RBD-His protein bands (ranging from 1.1 ng to 35.2 ng). The RBD antigen content in subcellular fractions was calculated by determining the integrated density values of electrophoretic bands from western blot analysis, applying the standard curve to quantify protein mass. The antigen content in subcellular components was further calculated by accounting for the volume ratios of subcellular fractions to the whole-cell lysate, as determined during the separation process. The RBD antigen content corresponding to 10<sup>7</sup> colony-forming units was calculated by multiplying the fraction volume ratio with the total optical density 600 nm of bacteria used for separation. The detailed calculations for RBD antigen content in cell wall and membrane fractions are provided in the Results and Supplementary Data 1 and Fig. 1.

### Flow cytometric detection of surface RBD expression on CW-rBCG::RBD

Recombinant BCG cells (~ 1 × 10<sup>9</sup>) were resuspended in 5 ml PBST-80 (PBS containing 0.05% Tween-80), washed twice, and resuspended in 1 ml PBST-80. Cells were incubated with the anti-RBD rabbit polyclonal antibody (same as used in the Western blot assay) at 4 °C for 2 h, followed by two washes with 2 ml PBST-80. The cell pellet was then incubated with FITC-conjugated goat anti-rabbit IgG secondary antibody (ABclonal, AS011) in the dark at room temperature for 1 h. After two additional washes with PBST-80, cells were resuspended in 2 mL PBST-80 and analyzed using flow cytometry (Beckman, DxFLEx).

### Immunization and euthanasia procedures for mice

All mouse experiments were conducted in accordance with the ARRIVE guidelines. Eight-week-old female BALB/c mice (SPF-grade) were purchased from Jiangsu Hua Chuang Xin Nuo Pharmaceutical Technology Co., Ltd. and randomly assigned to groups of six mice. All experiments were performed in two independent biological replicates, each using groups of six mice per condition. Where applicable, pooled sera or tissues were analyzed in technical duplicates or quadruplicates, as indicated in the figure legends. To evaluate different immunization routes, CW-rBCG::RBD was administered alone via intravenous (*i.v.*) or subcutaneous (*s.c.*) routes, or in combination with RBD<sup>AS01</sup> (10 µg RBD-His protein and 5 µg AS01 adjuvant). For intramuscular (*i.m.*) immunization, mice received two doses of RBD<sup>AS01</sup> at two-week or four-week intervals. For subcutaneous immunization, mice were primed with 1 × 10<sup>6</sup> cfu of either parent BCG or CW-rBCG::RBD (in 50 µl PBS per mouse) via two footpad injections. They were then vaccinated with one dose of RBD<sup>AS01</sup> via the intramuscular route, followed by a booster dose at week 2. For intravenous immunization alone, single low-dose CW-rBCG::RBD (1 × 10<sup>5</sup> cfu in 100 µl PBS per mouse) and standard-dose of CW-rBCG::RBD or BCG (1 × 10<sup>6</sup> cfu in 100 µl PBS per mouse) was skilled administered via tail vein injection. In the two-dose intravenous regimen, mice were primed with 1 × 10<sup>6</sup> cfu of either parent BCG or CW-rBCG::RBD (in 100 µl PBS per mouse) at four-week intervals. For intravenous immunization CW-rBCG::RBD or BCG, followed by two booster doses of RBD<sup>AS01</sup> at weeks 4 and 6. The PBS group served as the negative control. Blood samples were collected at weeks 6, 8, 16, and 31. At weeks 8 and 12, mice were euthanized via isoflurane inhalation. For euthanasia, 3 ml of isoflurane (97% vol/vol) was placed on a cotton ball in a desiccator-like glass container, and the desiccator-like glass container was sealed to allow the isoflurane to evaporate. The mice were placed inside the desiccator-like glass container and became unresponsive, indicating sufficient anesthesia. The mice were left in the desiccator-like glass container for 10 min for euthanasia, after which tissue sampling was performed. Spleen, lymph nodes, bone marrow, and lungs were harvested for immunological assays.

### Enzyme-Linked immunosorbent assays (ELISA)

Blood samples were collected and subsequently centrifuged at 3,000 rpm for 30 min at 4 °C. The resulting serum was carefully extracted and stored at -80 °C for subsequent neutralization assays and ELISAs. To evaluate the antibody response in mice immunized from various experimental groups, ELISA plates were coated overnight at 4 °C with 100 µl RBD-His protein (2.5 µg/ml). Following this, the plates were blocked using a blocking buffer consisting of PBS-Tween20 with 5% BSA, incubated at 37 °C for 2 h. After two washes with PBS-Tween20, serially diluted sera, starting from 1:100 with double fold increments, were added to the plates and incubated for 1 h at 37 °C. Following four washes, plates were incubated with HRP-conjugated goat anti-mouse IgG (Sigma, USA), polyclonal goat anti-mouse IgG1, polyclonal goat anti-mouse IgG2a, for 1 h at 37 °C. After four additional washes, the reaction was visualized by adding 3,3',5,5'-Tetramethylbenzidine (TMB), and then terminated with H<sub>2</sub>SO<sub>4</sub>. Absorbance at 450 nm was measured using a microplate reader (Infinite M200PRO, Switzerland). Titers were expressed as the reciprocal of the last dilution demonstrating an A450 value exceeding 2-fold of the PBS vaccination group values.

#### *Pseudotyped SARS-CoV-2 neutralization assay*

The SARS-CoV-2 pseudovirus was produced on HEK293 T cells as previously reported<sup>47</sup>. Briefly, the spike (GenBank: QHD43416) - encoding plasmid was co-transfected with the backbone plasmid pNL4-3.Luc.R-E with the proportion of 1:3 using Vigofect reagent. The supernatant of HEK293 T cells containing SARS-CoV-2 pseudovirus was harvested at 48 h post-transfection and used in the following neutralization assay. The assessment of pseudotyped SARS-CoV-2 (WT) neutralization adhered to previously established methodologies. Serum samples from mice were subjected to inactivation at 56 °C for 30 min. Huh-7 cells, seeded at a density of  $7 \times 10^3$  cells per well in a 96-well plate, were engaged in subsequent steps. Serum was initially diluted 1:100-fold with DMEM containing 1% penicillin-streptomycin, and then continued to be serially diluted for five concentration gradients at 3-fold dilutions. The equal volume of pseudotyped virus was co-incubated with diluted serum for 30 min. This serum-virus mixture was then transferred to Huh-7 cells. Following a 12 h incubation, the cell supernatants were replenished with fresh DMEM containing 10% FBS and cultured further for 48 h. Luciferase activity was gauged via a microplate reader (Infinite M200PRO, Switzerland), with neutralization titers ( $NT_{50}$ ) values determined as serum dilutions capable of diminishing luminescence units by 50% relative to virus control wells. Titers registering below 1:100 were deemed below the detectable threshold.

#### *Enzyme-Linked immunospot assay (ELISPOT)*

We detect the IFN- $\gamma$  positive T cells using ELISPOT assay. Specifically, ELISPOT plates were coated with Purified Anti-mouse IFN- $\gamma$  capture antibody and incubated overnight at 4 °C. After blocking,  $1 \times 10^5$  single lung cells from immunized mice were added per well and stimulated with SARS-CoV-2 RBD peptide pools for 44 h at 37 °C. Plates were washed, and spots corresponding to antigen-specific cytokine IFN- $\gamma$ -secreting cells were developed using BD ELISPOT AEC Substrate Set (551951). The chromogenic reaction was visualized and stopped, membrane was dried and the spots were counted and quantified using an Immunospot Reader (Champspot III, Beijing Sage Creation Science) to ensure procedural consistency and minimize errors throughout the experiment.

#### *Sample collection and processing and flow cytometry*

Flow cytometry served as the primary tool for assessing T cell populations in lung and spleen tissues. Single cells isolated from lung and spleen tissues were seeded at a density of  $2 \times 10^6$  cells per well in 96-well plates and cultured in RPMI 1640 medium supplemented with 10% heat-inactivated FBS and penicillin/streptomycin. Stimulation with 2.5  $\mu$ g/ml of RBD peptide pools was conducted for 42–44 h, with addition of Golgi Stop for the last 22–24 h. Sample collection involved swift isolation of spleens and lungs from euthanized mice, followed by submersion in cold RPMI 1640 medium containing 10% heat-inactivated FBS and 1% penicillin/streptomycin. Immediate processing of all organs ensued after collection. Spleens were homogenized using a syringe plunger and filtered through a 40  $\mu$ m cell strainer on ice. Red blood cells (RBCs) in spleens were lysed using ACK lysing buffer for 5–8 min on ice, with the reaction stopped using cold RPMI 1640 containing 10% FBS. Lungs were dissected into small pieces and incubated with 100  $\mu$ l *Collagenase IV* and 10  $\mu$ l *DNase I* at 37 °C for 30–45 min in a total volume of 50 ml, also filtered through a 40  $\mu$ m cell strainer on ice. RBC lysis was performed as described for spleens. Cells from all tissues were resuspended in ice-cold RPMI 1640 medium and immediately counted using a Count Star cell counter (IC1000, USA) to achieve a concentration of  $2 \times 10^7$  cells/ml. Bone marrow (BM) was flushed from both femurs and tibias of each mouse using a 5 ml 25 G syringe. The samples were pooled, and red blood cells were lysed using ACK lysing buffer (Beyotime Biotechnology, C3702) for 5–8 min on ice. Following lysis, the cell concentration was adjusted to  $2 \times 10^7$  cells/ml using a Count Star cell counter (IC1000, USA). For the generation of the RBD fluorescent probe, RBD-His protein used in flow cytometry experiments was conjugated to Alexa Fluor 647 using the Alexa Fluor<sup>®</sup> 647 Conjugation Kit (Abcam, 269823) according to the manufacturer's instructions. Subsequently, the samples were cultured in RPMI 1640 medium containing 10% heat-inactivated FBS and 1% penicillin/streptomycin. The samples were incubated with 2.5  $\mu$ g/ml RBD peptide pools for 44 h. To assess IFN- $\gamma$  secretion, Golgi Plug (BD Biosciences, 555029) was added to the medium for the final 3 h of incubation prior to staining. All staining steps were carried out at 4 °C in FACS buffer (PBS with 2% heat-inactivated FBS). Single cell suspensions were blocked with anti-CD16/CD32 monoclonal antibody (mouse BD Fc block) prior to staining. Fixable Viability Stain 780 was applied for 30 min, followed by surface staining supplemented with Brilliant Stain buffer (BD Bioscience, 563794). Subsequently, cells were washed with FACS buffer, fixed, and permeabilized with Cytofix/Cytoperm solution according to the manufacturer's instructions for 30 min, followed by incubation with intracellular antibody panels. After washing, cells were resuspended in 2% FBS solution in PBS buffer for flow cytometry analysis. All samples were acquired using an LSRFortessa flow cytometer (BD Biosciences) and analyzed using FlowJo version10 (Treestar).

#### *Key resources table*

Antibodies	fluorescence	dilution	source	Cat#
Live/Dead	FVS780	1:2000	BD	565388
Fc Block	N/A	1:300	BD	553141
CD3	BUV395	1:250	BD	563565
CD4	BV421	1:200	BD	562891
CD8	BV711	1:200	BD	563,046
CXCR5	Percyp-cy5.5	1:200	Biolegend	566493
PD-1	BV605	1:200	BD	563059

Antibodies	fluorescence	dilution	source	Cat#
CD44	BV480	1:200	BD	566200
CD62L	APC	1:200	BD	561919
CD11a	BUV496	1:200	BD	741056
GL7	FITC	1:200	BD	562080
B220	AF700	1: 200	BD	557963
IgG2a	PE	1: 200	Biolegend	407108
IgD	PE-Cy7	1: 200	Biolegend	405719

SARS-CoV-2 RBD peptide pool	Sino, China	PP002
SARS-CoV-2 RBD-His protein	Easy Biotech, China	2020 T4

### Ethics statement

All animal experiments were approved by the Institutional Animal Care and Use Committee (IACUC) and the Ethics Committee of the Shanghai Public Health Clinical Center Laboratory Animal Welfare (Protocol No. 2021-A063-02). All methods were performed in accordance with relevant institutional guidelines, national regulations, and the ARRIVE guidelines. Mice were euthanized using isoflurane inhalation in accordance with the AVMA Guidelines for the Euthanasia of Animals (2020).

### Statistical analysis

Statistical analysis and graph generation were performed using GraphPad Prism 9.0. The display of the results and the drawing of the schematic diagram are done by Adobe Illustrator 2024. Data are presented as mean  $\pm$  SEM. The Student's *t*-tests was used for comparisons between two independent groups, ordinary one-way ANOVA was used for multiple group comparisons. With a 5% significance level. *p*-values are indicated in the graphs. The precise number of samples analyzed in each graph is reported in figure captions.

### Data availability

All data supporting the findings of this study are included in this manuscript or supplementary file. All relevant data are available from the corresponding authors upon reasonable request.

Received: 16 February 2025; Accepted: 29 April 2025

Published online: 16 May 2025

### References

- Begnini, K. R., Buss, J. H., Collares, T. & Seixas, F. K. Recombinant Mycobacterium bovis BCG for immunotherapy in nonmuscle invasive bladder cancer. *APPL. MICROBIOL. BIOT.* **99**, 3741 (2015).
- Yuan, S. et al. Immunization with two Recombinant Bacillus Calmette–Guerin vaccines that combine the expression of multiple tandem repeats of mucin-1 and colony stimulating-factor suppress breast tumor growth in mice. *J. CANCER RES. CLIN.* **136**, 1359 (2010).
- Kato, S. et al. CD8 T cells show protection against highly pathogenic Simian immunodeficiency virus (SIV) after vaccination with SIV Gene-Expressing BCG prime and vaccinia virus/Sendai virus vector boosts. *J. VIROL.* **95** (2021).
- Uno-Furuta, S. et al. Immunization with recombinant Calmette-Guerin bacillus (BCG)-hepatitis C virus (HCV) elicits HCV-specific cytotoxic T lymphocytes in mice. *VACCINE* **21** 3149 (2003).
- Bueno, S. M. et al. Protective T cell immunity against respiratory syncytial virus is efficiently induced by recombinant BCG. *Proceedings of the National Academy of Sciences - PNAS* **105** 20822 (2008).
- Chapman, R., Chege, G., Shephard, E., Stutz, H. & Williamson, A. L. Recombinant Mycobacterium bovis BCG as an HIV vaccine vector. *CURR. HIV RES.* **8**, 282 (2010).
- Palavecino, C. E., Céspedes, P. E., Gómez, R. S., Kalergis, A. M. & Bueno, S. M. Immunization with a recombinant bacillus Calmette-Guerin strain confers protective Th1 immunity against the human metapneumovirus. *The Journal of immunology (J)* **192** 214 (2014). (1950).
- Rey-Jurado, E., Soto, J., Gálvez, N. & Kalergis, A. M. A safe and efficient BCG vectored vaccine to prevent the disease caused by the human Respiratory Syncytial Virus. *HUM VACC IMMUNOTHER* **13** (2017). (2092).
- Kaufmann, S. H. E. Envisioning future strategies for vaccination against tuberculosis. *Nat. Reviews: Immunol.* **6**, 699 (2006).
- Counoupas, C. et al. A single dose, BCG-adjuvanted COVID-19 vaccine provides sterilising immunity against SARS-CoV-2 infection. *NPJ VACCINES.* **6**, 143 (2021).
- Vinuesa, C. G., Linterman, M. A., Yu, D. & MacLennan, I. C. Follicular helper T cells. *ANNU. REV. IMMUNOL.* **34**, 335 (2016).
- Crotty, S. & Follicular Helper, T. Cell differentiation, function, and roles in disease. *IMMUNITY* **41**, 529 (2014).
- Li, W. et al. Prime-boost vaccination with Bacillus calmette Guerin and a Recombinant adenovirus co-expressing CFP10, ESAT6, Ag85A and Ag85B of Mycobacterium tuberculosis induces robust antigen-specific immune responses in mice. *MOL. MED. REP.* **12**, 3073 (2015).
- Ramírez, M. A. et al. Co-administration of Recombinant BCG and SARS-CoV-2 proteins leads to robust antiviral immunity. *VACCINE* **42**, 126203 (2024).
- Sartain, M. J. & Belisle, J. T. N-Terminal clustering of the O-glycosylation sites in the Mycobacterium tuberculosis lipoprotein SodC. *Glycobiology (Oxford)*. **19**, 38 (2009).
- Malen, H., Pathak, S., Softeland, T., de Souza, G. A. & Wiker, H. G. Definition of novel cell envelope associated proteins in Triton X-114 extracts of Mycobacterium tuberculosis H37Rv. *BMC MICROBIOL.* **10**, 132 (2010).
- Yang, E. et al. Recombinant BCG prime and PPE protein boost provides potent protection against acute Mycobacterium tuberculosis infection in mice. *MICROB. PATHOGENESIS.* **93**, 1 (2016).

18. Neyrolles, O. et al. Lipoprotein access to MHC class I presentation during infection of murine macrophages with live mycobacteria. *J. IMMUNOL.* **166**, 447 (2001).
19. Greenaway, C. et al. Humoral response to Mycobacterium tuberculosis antigens in patients with tuberculosis in the Gambia. *INT. J. TUBERC LUNG D.* **9**, 1112 (2005).
20. La Manna, M. P. et al. Impact of Mycobacterium tuberculosis Infection on Human B Cell Compartment and Antibody Responses. *CELLS-BASEL* **11** 2906 (2022).
21. Maeda, F. Y. et al. Surface-associated antigen induces permeabilization of primary mouse B-cells and lysosome exocytosis facilitating antigen uptake and presentation to T-cells. *ELIFE* **10** (2021).
22. Oftung, F., Mustafa, A. S., Husson, R., Young, R. A. & Godal, T. Human T cell clones recognize two abundant Mycobacterium tuberculosis protein antigens expressed in Escherichia coli. *J. IMMUNOL.* **138**, 927 (1987).
23. Bothamley, G. H. Epitope-specific antibody levels demonstrate recognition of new epitopes and changes in titer but not affinity during treatment of tuberculosis. *Clin. Diagn. Lab. Immunol.* **11**, 942 (2004).
24. *The Comprehensive Sourcebook of Bacterial Protein Toxins (Fourth Edition)* (ACADEMIC, p. 77. (2015).
25. Helenius, A. & Simons, K. Solubilization of membranes by detergents. *Biochim. Biophys. Acta.* **415**, 29 (1975).
26. Helenius, A., McCaslin, D. R., Fries, E. & Tanford, C. (Elsevier Science & Technology, United States, Vol. 56, p. 734. (1979).
27. Young, D. B. & Garbe, T. R. Lipoprotein antigens of Mycobacterium tuberculosis. *RES. MICROBIOL.* **142**, 55 (1991).
28. Hu, Z. et al. A two-dose optimum for Recombinant S1 protein-based COVID-19 vaccination. *VIROLOGY* **566**, 56 (2022).
29. Lederer, K. et al. SARS-CoV-2 mRNA Vaccines Foster Potent Antigen-Specific Germinal Center Responses Associated with Neutralizing Antibody Generation. *IMMUNITY* **53** 1281 (2020).
30. Basile, J. I. et al. Mycobacteria-Specific T cells are generated in the lung during mucosal BCG immunization or infection with Mycobacterium tuberculosis. *FRONT. IMMUNOL.* **11** (2020).
31. Tarke, A. et al. SARS-CoV-2 vaccination induces immunological T cell memory able to cross-recognize variants from Alpha to Omicron. *CELL* **185** 847 (2022).
32. Darrah, P. A. et al. Prevention of tuberculosis in macaques after intravenous BCG immunization. *NATURE* **577**, 95 (2020).
33. Stevens, T. L. et al. Regulation of antibody isotype secretion by subsets of antigen-specific helper T cells. *NATURE* **334**, 255 (1988).
34. Bornstein, G. G., Klakamp, S. L., Andrews, L., Boyle, W. J. & Tabrizi, M. Surrogate approaches in development of monoclonal antibodies. *DRUG DISCOV TODAY.* **14**, 1159 (2009).
35. Ewer, K. J. et al. T cell and antibody responses induced by a single dose of ChAdOx1 nCoV-19 (AZD1222) vaccine in a phase 1/2 clinical trial. *NAT. MED.* **27**, 270 (2021).
36. Juno, J. A. et al. Humoral and Circulating follicular helper T cell responses in recovered patients with COVID-19. *NAT. MED.* **26**, 1428 (2020).
37. Hilligan, K. L. et al. Intravenous administration of BCG protects mice against lethal SARS-CoV-2 challenge. *J. EXP. MED.* **219** (2022).
38. Singh, S., Saavedra-Avila, N. A., Tiwari, S. & Porcelli, S. A. A century of BCG vaccination: immune mechanisms, animal models, non-traditional routes and implications for COVID-19. *FRONT. IMMUNOL.* **13** (2022).
39. Podaza, E. et al. Evaluation of T-Cell responses against shared melanoma associated antigens and predicted neoantigens in cutaneous melanoma patients treated with the CSF-470 allogeneic cell vaccine plus BCG and GM-CSF. *FRONT. IMMUNOL.* **11** (2020).
40. Gruell, H. et al. Antibody-mediated neutralization of SARS-CoV-2. *IMMUNITY* **55** 925 (2022).
41. Iwasaki, A. Exploiting mucosal immunity for antiviral vaccines. *ANNU. REV. IMMUNOL.* **34**, 575 (2016).
42. Zhang, B. et al. Bacillus Calmette-Guérin-induced trained immunity protects against SARS-CoV-2 challenge in K18-hACE2 mice. *JCI Insight* **7** (2022).
43. Peralta Alvarez, M. P. et al. Low-dose M.tb infection but not BCG or MTBVAC vaccination enhances heterologous antibody titres in non-human primates. *FRONT. IMMUNOL.* **15** (2024).
44. Cirovic, B. et al. Vaccination in humans elicits trained immunity via the hematopoietic progenitor compartment. *CELL. HOST MICROBE.* **28**, 322 (2020).
45. Kong, L. et al. Single-cell transcriptomic profiles reveal changes associated with BCG-induced trained immunity and protective effects in Circulating monocytes. *CELL. REP.* **37**, 110028 (2021).
46. Ziogas, A. & Netea, M. G. Trained immunity-related vaccines: innate immune memory and heterologous protection against infections. *TRENDS MOL. MED.* **28**, 497 (2022).
47. Liu, Z. et al. A novel STING agonist-adjuvanted pan-sarbecovirus vaccine elicits potent and durable neutralizing antibody and T cell responses in mice, rabbits and NHPs. *CELL. RES.* **32**, 269 (2022).

## Acknowledgements

This research was funded by the National Key R&D Program of China (2023YFC2307303 to L.D.L.); the National Natural Science Foundation (82372293 and 31970032 to L.D.L., 31830002 to G.P. Z., and 82171815 to F.X.Y.); the Shanghai Municipal Health Commission (2024ZZ2009 to Z.D.H.); the Shanghai Disease Control and Prevention Administration (2024GKM34 to Z.D.H.); and the Science and Technology Commission of Shanghai Municipality (ZD2021 CY001 to L.D.L.).

## Author contributions

J.Y.Z., Z.D.H., X.Y.F., L.D.L. and G.P.Z. conceived this project and designed the experiments. J.Y.Z., L.X.X., Z.D.H., Z.Y.C., J.C.X., Q.Y.W. and J.W. performed the experiments; L.X.X. performed neutralizing antibody testing; J.Y.Z., Z.Y.C., J.C.X., Q.Y.W. and J.W. collected mouse serum and immune tissues and prepared single-cell samples; J.Y.Z. performed cellular immunological analysis; J.Y.Z., Z.D.H. and L.D.L. wrote and edited the manuscript. L.D.L. supervised the project. All authors reviewed the manuscript.

## Declarations

## Competing interests

The authors declare no competing interests.

## Additional information

**Supplementary Information** The online version contains supplementary material available at <https://doi.org/10.1038/s41598-025-00553-x>.

**Correspondence** and requests for materials should be addressed to G.-P.Z., X.-Y.F. or L.-D.L.

**Reprints and permissions information** is available at [www.nature.com/reprints](http://www.nature.com/reprints).

**Publisher's note** Springer Nature remains neutral with regard to jurisdictional claims in published maps and institutional affiliations.

**Open Access** This article is licensed under a Creative Commons Attribution-NonCommercial-NoDerivatives 4.0 International License, which permits any non-commercial use, sharing, distribution and reproduction in any medium or format, as long as you give appropriate credit to the original author(s) and the source, provide a link to the Creative Commons licence, and indicate if you modified the licensed material. You do not have permission under this licence to share adapted material derived from this article or parts of it. The images or other third party material in this article are included in the article's Creative Commons licence, unless indicated otherwise in a credit line to the material. If material is not included in the article's Creative Commons licence and your intended use is not permitted by statutory regulation or exceeds the permitted use, you will need to obtain permission directly from the copyright holder. To view a copy of this licence, visit <http://creativecommons.org/licenses/by-nc-nd/4.0/>.

© The Author(s) 2025